Aerodynamic Heating on 3-D Bodies Including the Effects of Entropy-Layer Swallowing

FRED R. DEJARNETTE*
North Carolina State University, Raleigh, N.C.
AND
H. HARRIS HAMILTON†
NASA Langley Research Center, Hampton, Va.

A relatively simple method is presented to include the effects of entropy-layer swallowing in a method developed previously for calculating laminar, transitional, and turbulent heating rates on three-dimensional bodies in hypersonic flows. The boundary layer swallows the entropy layer when the boundary layer downstream of the nose region has entrained those streamlines which passed through the nearly normal part of the bow shock wave. The entropy at the edge of the boundary layer is then determined by equating the mass flow inside the boundary layer to that entering part of the bow shock wave. A new inviscid flowfield solution, which is an extension of Maslen's axisymmetric method, is developed to calculate the three-dimensional shock shape and couple the inviscid solution with the viscous solution. The calculated heating rates compare favorably with Mayne's theory and experimental data for blunted circular and elliptical cones at angles of attack. The effects of entropy layer swallowing on the calculated heating rates were small for laminar heating but large increases were noted for the turbulent heating rates. The computer program developed to calculate the results presented herein required only about 7 sec per streamline on the IM 370/165 computer.

Nomenclature

B = ratio of body principal radii of curvature, R_T/R_{11}
$\bar{B}$ = ratio of shock principal radii of curvature, $\bar{R}_T/\bar{R}_{11}$
$\bar{C}$ = parameter used in Eq. (23)
$\bar{C}'$ = $d\bar{C}/d\bar{\beta}$
D = constant defined by Eq. (41a)
$\hat{\mathbf{e}}_{\bar{s}}, \hat{\mathbf{e}}_{\bar{\beta}}, \hat{\mathbf{e}}_{\bar{n}}$ = unit vectors in shock-oriented coordinate system
$\hat{\mathbf{e}}_{\bar{x}}, \hat{\mathbf{e}}_{\bar{y}}, \hat{\mathbf{e}}_{\bar{z}}$ = unit vectors in wind-oriented Cartesian coordinate system
E = constant defined by Eq. (41b)
G^2 = $1-\sin^2\bar{\Gamma}$
h = scale factor in β-direction on body
$\bar{h}$ = scale factor in $\bar{\beta}$-direction on shock
$\bar{h}_s$ = scale factor in $\bar{\xi}$ direction on shock, $d\bar{S} = \bar{h}_s d\bar{\xi}$
h_c = heat transfer coefficient, Btu/ft^2-sec-°R
h_w = wall enthalpy
h_2 = enthalpy aft of normal shock
Δh = enthalpy parameter defined by Eq. (33)
H_s = stagnation enthalpy
M = Mach number
n = distance normal to a streamline
$\bar{n}$ = straight line coordinate normal to shock wave and toward body
p = pressure
Δp = pressure parameter defined by Eq. (32)
q_w = heat-transfer rate at wall
R = streamline radius of curvature
$\bar{R}$ = shock radius of curvature along $\bar{\beta}$ = constant line, see Eq. (10)
$Re_{\infty,N}$ = freestream Reynolds number based on nose radius
R_N = nose radius
R_T, R_{11} = body principal radii of curvature at stagnation point
$\bar{R}_T, \bar{R}_{11}$ = shock principal radii of curvature at stagnation line
S = distance along inviscid surface streamline
$\bar{S}$ = distance along $\bar{\beta}$ = constant line on shock
St = Stanton number based on freestream conditions and a recovery factor of unity
$S\text{-}C$ = Spalding-Chi method
$\bar{u}, \bar{v}, \bar{w}$ = velocity components in $\bar{\xi}$, $\bar{n}$, and $\bar{\beta}$ directions, respectively
V = velocity magnitude
$\mathbf{V}$ = velocity vector
$V\text{-}D\ II$ = Van Driest II method
x, y, z = body-oriented coordinate system
$\bar{x}, \bar{y}, \bar{z}$ = Cartesian coordinates in wind-oriented coordinate system with origin at the stagnation line of shock wave, see Fig. 3
α = angle of attack
β = body coordinate normal to inviscid surface streamline
$\bar{\beta}$ = shock coordinate normal to $\bar{\xi}$ lines
γ = ratio of specific heats
$\bar{\Gamma}$ = shock-wave angle (see Fig. 4)
δ = boundary-layer thickness
δ^* = boundary-layer displacement thickness
Δ = shock standoff distance
η = Ψ/Ψ_{sh}
Λ = exponent defined by Eq. (38)
$\bar{\xi}$ = coordinate along shock surface
ρ = mass density
$\bar{\sigma}$ = angle measured on shock wave, see Eq. (15) and Fig. 4
ϕ = body circumferential angle with $\phi = 0$ in windward plane of symmetry
$\bar{\phi}$ = shock circumferential angle, $\bar{\phi} = \tan^{-1}(\bar{z}/\bar{y})$
Φ = second stream function, see Eq. (1)
Ψ = first stream function, see Eq. (1)

Subscripts

b = body
$B.L.$ = boundary layer
e = edge of boundary layer
s = stagnation point
sh = at shock wave
w = wall
2 = aft of normal shock
∞ = freestream conditions

Presented as Paper 74-602 at the AIAA 7th Fluid and Plasma Dynamics Conference, Palo Alto, Calif., June 17–19, 1974; submitted July 1, 1974; revision received October 4, 1974. This research was supported by Contract NAS1-10277, NASA Langley Research Center.

Index categories: Boundary Layers and Convective Heat Transfer—Laminar; Boundary Layers and Convective Heat Transfer—Turbulent; Supersonic and Hypersonic Flow.

* Professor of Mechanical and Aerospace Engineering, Associate Fellow AIAA.

† Aerospace Engineer, Aerothermal Branch, Space Systems Division.

Introduction

A RELATIVELY simple method was developed previously[1] for calculating laminar, transitional, and turbulent heating rates on three-dimensional bodies in hypersonic flows. Inviscid surface streamlines were calculated from Euler's equation using

a prescribed pressure distribution. Heating rates were then determined along a streamline by applying the axisymmetric analog or small cross-flow approximation to the three-dimensional boundary-layer equations. This method was shown to yield reasonably accurate results for laminar heating on blunted circular and elliptical cones and an earlier version of the space shuttle vehicle. However, properties at the edge of the boundary layer were determined from the surface pressure and the entropy aft of a normal shock wave (typical blunt body assumption). Although this assumption is valid for high Reynolds numbers and in the nose region of blunt bodies, its accuracy decreases downstream of the stagnation region. As the boundary layer along the surface grows, more and more of the inviscid-flow mass is entrained into the boundary layer, and the streamlines which passed through the nearly normal portion of the bow shock wave are "swallowed" by the boundary layer. This phenomenon is often referred to as entropy-layer or streamline swallowing, and it can have a significant effect on the calculated heating rates. To account for these effects the viscous flowfield must be coupled with an inviscid flowfield solution.

The problem of entropy-layer swallowing by the boundary layer has been treated by many investigators for the special cases of two-dimensional and axisymmetric flows.[2-4] In the classical treatment, neglecting entropy-layer swallowing, the outer-edge conditions for the boundary-layer equations are assumed to be the conditions of the inviscid flowfield on the body surface. This is equivalent to assuming that all of the fluid along the outer edge of the boundary layer crossed the normal portion of the bow shock wave. However, Fig. 1 illustrates how the boundary layer can "swallow" that portion of the fluid which crossed the nearly normal part of the shock (entropy layer). When this occurs, the streamline at the edge of the boundary layer will have passed through an oblique part of the shock wave and hence the entropy of this streamline differs from normal-shock entropy. Although the pressure at the boundary-layer edge is nearly the same as the surface pressure, the other fluid properties are quite different from those assuming the edge streamline passed through a normal shock wave. Entropy-layer swallowing has been shown to significantly affect heating rates and skin friction.[2-4]

For three-dimensional flows, the relatively simple mass-balance method for treating entropy-layer swallowing in axisymmetric flows can no longer be used because the streamlines wrap around the body and destroy the axial symmetry. Mayne[5,6] has considered the effects of entropy-layer swallowing on the boundary layers of sharp circular cones at angles of attack and also the windward plane of symmetry on blunted circular cones at angles of attack. He used a finite-difference technique for solving the three-dimensional boundary-layer equations. For the inviscid flowfield calculations he used Jones' method[7] for sharp cones at an angle of attack, and a combination of an inverse method and Rakich's three-dimensional method of characteristics[8] for the blunted cones. A scheme is developed to account for entropy-layer swallowing by a local mass-flow balance between the boundary-layer flow and the entrained inviscid flow. Mayne's results compared favorably with experimental data for both laminar and turbulent heating rates.

This paper develops an approximate method to include entropy-layer swallowing in the heating rates calculated by the method of Ref. 1. In that method laminar heating-rates were computed by applying the axisymmetric analog to the local similarity method of Beckwith and Cohen[9] and turbulent heating-rates from Spalding and Chi's method[10] coupled with a modified form of Reshotko and Tucker's integral method.[11] Transitional heating rates were calculated from a weighted sum[12] of the local laminar and turbulent heating rates. In order to keep the computations short and simple, the three-dimensional inviscid flowfield is calculated here by a new, approximate method which is an extension of Maslen's method for axisymmetric flows.[13] Although this method is not as accurate as Mayne's technique,[5,6] the present method is applicable to the entire flowfield of three-dimensional bodies whereas Mayne's method is restricted to pointed circular cones and the windward plane of symmetry for blunt-nosed axisymmetric bodies. Results presented in this paper are for an ideal gas; however, both ideal gas and equilibrium air properties are included in the present analysis.

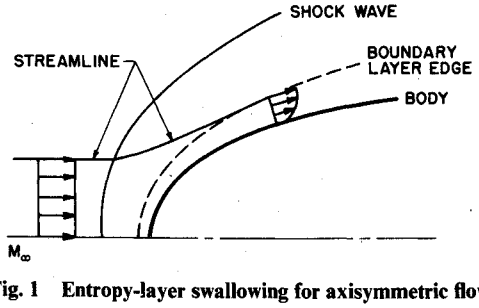

Fig. 1 Entropy-layer swallowing for axisymmetric flow.

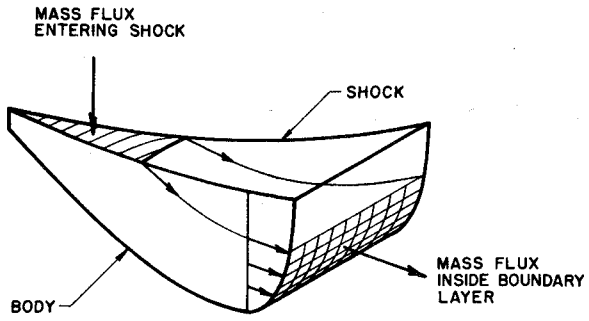

Fig. 2 Entropy-layer swallowing for a segment of a 3-D flow.

Analysis

To account for entropy-layer swallowing, the position where the streamline at the edge of the boundary layer passed through the bow shock wave is located by balancing the mass flow which entered a segment of the shock wave with that inside the boundary layer (see Fig. 2). Then the slope of the shock wave at that position determines the entropy of that streamline and hence the entropy at the edge of the boundary layer. Therefore, for the purposes of this paper the shape of the shock wave must be determined but the complete three-dimensional flowfield is not needed. The analysis presented here is given in more detail in Ref. 15.

Inviscid Flowfield

In 1964 Maslen[13] developed a simple method for calculating the inviscid flowfield over smooth axisymmetric bodies. It is an inverse method based on the use of von Mises transformation coupled with a simple approximate integral of the momentum equation normal to the shock wave. Although approximate, the technique is easy to apply and yields accurate results. More recently Maslen[14] extended this method to asymmetric flows and presented results for the stagnation region of blunt bodies and for conical bodies. However, that method is much more complicated than the axisymmetric method, and it is rather cumbersome to apply. Moreover, the shock standoff distance at the stagnation line was found to be different for different directions of approaching the stagnation line. The method developed here represents an extension of Maslen's earlier axisymmetric method[13] to general three-dimensional flows, but it is much simpler and easier to apply than Maslen's more recent asymmetric method.[14]

For three-dimensional flows the continuity equation is automatically satisfied by introducing a pair of stream functions, Ψ and Φ, such that

$$-\rho \mathbf{V} = \nabla\Psi \times \nabla\Phi \tag{1}$$

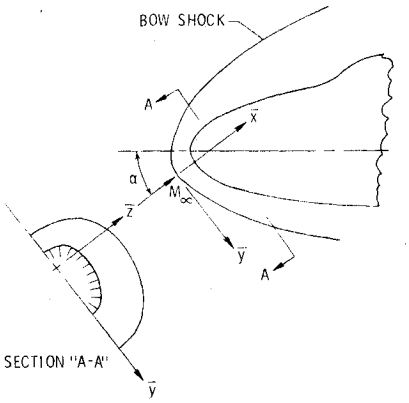

Fig. 3 Shock-oriented coordinate system.

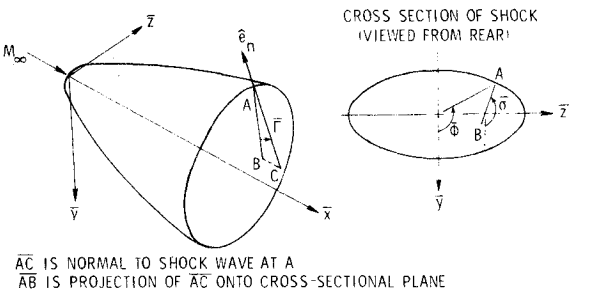

Fig. 4 Geometry of shock-wave angles $\bar{\Gamma}$ and $\bar{\sigma}$.

Intersections of constant Ψ surfaces with constant Φ surfaces are streamlines; however, there is a certain arbitrariness in the definition of the two stream functions in that they are not unique. The second stream function, Φ, is chosen so that it reduces to the circumferential angle $\bar{\phi}$ for the special case of axisymmetric flow. Constant Φ surfaces are normal to the shock wave, and at the shock surface the plane tangent to a constant Φ surface contains the velocity vector. Thus the velocity component tangent to the shock wave, which does not change across the shock, is tangent to the curve generated by the intersection of a constant Φ surface with the shock surface.‡ No approximations are involved in this choice of the second stream function Φ. However, it is assumed that inside the shock layer the constant Φ surfaces contain generators which are straight lines normal to the shock wave. Thus these surfaces have the correct shape and slope at the shock wave, but they are not constrained to satisfy all the flowfield equations inside the shock layer. However, as pointed out by Maslen,[14] for blunt bodies in hypersonic flow the majority of the mass flow tends to be thrown toward the shock wave with low density near the body. Hence the present method should calculate a reasonably accurate body shape corresponding to a given shock shape, although the direction of the velocity near the body may be in error. These arguments are substantiated, at least for conical bodies, by the numerical results.[14]

A shock-oriented, orthogonal coordinate system $\bar{\xi}$, $\bar{n}$, $\bar{\beta}$ is defined with $\bar{\xi}$ along the intersection of a constant Φ surface with the shock wave, $\bar{n}$ the straight-line distance normal (inward) to the shock wave, and $\bar{\beta}$ normal to $\bar{\xi}$ on the shock surface (see Figs. 3 and 4). The elemental arc lengths along these three coordinates are $d\bar{S} = h_s d\bar{\xi}$, $d\bar{n}$, and $\bar{h}\,d\bar{\beta}$, respectively, where $\bar{h}_s$ and $\bar{h}$ are the scale factors for the $\bar{\xi}$ and $\bar{\beta}$ coordinates, respectively. Let the velocity components in the $\bar{\xi}$, $\bar{n}$, and $\bar{\beta}$ directions be $\bar{u}$, $\bar{v}$, and $\bar{w}$, respectively. Since constant Φ surfaces intersect the shock surface along $\bar{\xi}$-curves and are assumed to contain the coordinate $\bar{n}$, then $\Phi \equiv \bar{\beta}$ and $\bar{w} \equiv 0$ inside the shock layer. Using these results Eq. (1) gives

$$\rho\bar{u}\bar{h} = -\partial\Psi/\partial\bar{n} \tag{2}$$

and

$$\rho\bar{v}\bar{h} = \partial\Psi/\partial\bar{S} \tag{3}$$

Equation (2) can be integrated across the shock layer to give

$$\bar{n} = (1/\bar{h})\int_{\Psi}^{\Psi_{sh}} (d\Psi/\rho\bar{u}) \tag{4}$$

and the body corresponds to $\Psi = 0$ and $\bar{n} = \Delta$. Equation (3) may be integrated in the $\bar{\xi}$-direction along the shock surface to give

$$\Psi_{sh} = \int_0^{\bar{S}} \rho\bar{v}\bar{h}\,d\bar{S} = \rho_\infty V_\infty \int_0^{\bar{S}} \sin\bar{\Gamma}\bar{h}\,d\bar{S} \tag{5}$$

where $\bar{\Gamma}$ is the shock-wave angle (see Fig. 4).

‡ These curves are paths of steepest descent on the shock surface, and they emanate from the stagnation line.

The momentum equation normal to a streamline is

$$\partial p/\partial n = -\rho V^2/R \tag{6}$$

As in Ref. 13, the streamlines are assumed to run parallel to the shock wave and; therefore $V \simeq \bar{u}$, $R \simeq \bar{R}$, and $n \simeq \bar{n}$. Now make a von Mises transformation so that the independent variables are $\bar{S}$ and Ψ in a constant $\bar{\beta}$ surface. With the aid of Eq. (2), Eq. (6) then becomes

$$\partial p/\partial\Psi = \bar{u}/(\bar{h}\bar{R}) \tag{7}$$

Finally assume $\bar{u}/(\bar{h}\bar{R})$ is constant across the shock layer and equal to its value on the shock wave. Then Eq. (7) becomes§

$$\partial p/\partial\Psi = \bar{u}_{sh}/(\bar{h}\bar{R}) \tag{8}$$

Equation (8) integrates to

$$p(\bar{\xi},\bar{\beta},\Psi) = p_{sh}(\bar{\xi},\bar{\beta}) + \frac{u_{sh}(\bar{\xi},\bar{\beta})\Psi_{sh}}{\bar{R}\bar{h}}\left(\frac{\Psi}{\Psi_{sh}} - 1\right) \tag{9}$$

where

$$\bar{R} \equiv -1/(\partial\bar{\Gamma}/\partial\bar{S}) \tag{10}$$

is the shock radius of curvature in $\bar{\xi}$ direction. The distinction between $p_{sh}(\bar{\beta},\Psi)$ and $p_{sh}(\bar{\xi},\bar{\beta})$ should be noted in Fig. 5. At any position $\bar{\xi}$, Ψ, $\bar{\beta}$ inside the shocklayer, Eq. (9) gives the pressure, and the entropy for that streamline is determined from the shock-wave angle where that streamline crossed the shock wave. At that position Ψ_{sh} given by Eq. (5) is equal to value of Ψ inside the shock layer. Then, with the pressure and entropy known, the density ρ and enthalpy h_e can be calculated from an equation of state for a perfect gas or a gas in equilibrium. Finally, the velocity $\bar{u}$ follows from the approximate energy equation

$$\bar{u} = [2(h_2 - h_e)]^{1/2} \tag{11}$$

which again is the same approximation used by Maslen. The physical location $\bar{n}$ of the streamline from the shock wave can be calculated by quadrature from Eq. (4). This method can be used to determine the flowfield properties across the shock layer at prescribed positions along a constant Φ surface, and then as many of these surfaces as required may be calculated to obtain an adequate distribution. Unlike Maslen's asymmetric method,[14] the solution here for each constant Φ surface can be calculated independently of other Φ = constant surfaces, which highly simplifies the calculations.

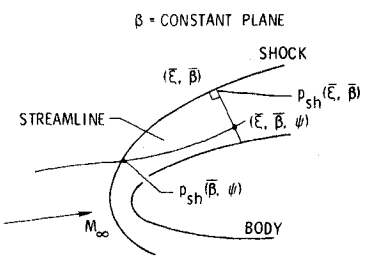

Fig. 5 Shock pressures and coordinate positions; $\bar{\beta}$ = constant plane.

§ As noted by Maslen,[13] the assumptions leading to Eq. (8) introduce compensating errors, and the resulting pressure equation is accurate except near the stagnation line.

Stagnation Region

For the stagnation region, it is convenient to use wind-oriented Cartesian coordinates $\bar{x}, \bar{y}, \bar{z}$ whose origin is located at the normal position on the shock wave with $\bar{x}$ in the direction of $\mathbf{V}_\infty$ (see Fig. 3). The shape of the shock wave near the stagnation line is represented by an elliptic paraboloid

$$\bar{x} = (\bar{y}^2/\bar{R}_{11} + \bar{z}^2/\bar{R}_T)/2 \tag{12}$$

where the $\bar{x}, \bar{y}$ plane is a plane of symmetry. At the origin, the principal shock radii of curvature are $\bar{R}_{11}$ in the $\bar{x}, \bar{y}$ plane and $\bar{R}_T$ in the $\bar{x}, \bar{z}$ plane.

The unit (outer) normal to the shock surface is illustrated in Fig. 4 and is given by the relation

$$\hat{\mathbf{e}}_{\bar{n}} = \sin\bar{\Gamma}(-\hat{\mathbf{e}}_{\bar{x}} + \bar{y}\hat{\mathbf{e}}_{\bar{y}}/\bar{R}_{11} + \bar{z}\hat{\mathbf{e}}_{\bar{z}}/\bar{R}_T) \tag{13}$$

where the slope of the shock wave with respect to the freestream velocity (shock-wave angle) is $\bar{\Gamma}$, and

$$\sin\bar{\Gamma} = [1 + (\bar{y}/\bar{R}_{11})^2 + (\bar{z}/\bar{R}_T)^2]^{-1/2} \tag{14}$$

In an $\bar{x}$ = constant plane, the angle $\bar{\sigma}$ on the shock wave (see Fig. 4) is defined by

$$\tan\bar{\sigma} = \bar{z}/(\bar{B}\bar{y}) \tag{15}$$

where

$$\bar{B} = \bar{R}_T/\bar{R}_{11} \tag{16}$$

Using Eqs. (14) and (15), Eq. (13) can also be written as

$$\hat{\mathbf{e}}_{\bar{n}} = -\sin\bar{\Gamma}\hat{\mathbf{e}}_{\bar{x}} + \cos\bar{\Gamma}(\cos\bar{\sigma}\hat{\mathbf{e}}_{\bar{y}} + \sin\bar{\sigma}\hat{\mathbf{e}}_{\bar{z}}) \tag{17}$$

With $\hat{\mathbf{e}}_{\bar{s}}$ and $\hat{\mathbf{e}}_{\bar{\beta}}$ unit vectors in the $\bar{\xi}$ and $\bar{\beta}$ directions, the direction of $\hat{\mathbf{e}}_{\bar{s}}$ which makes $\bar{w} = 0$ at the shock surface is obtained from the shock relations as

$$\hat{\mathbf{e}}_{\bar{s}} = \cos\bar{\Gamma}\hat{\mathbf{e}}_{\bar{x}} + \sin\bar{\Gamma}(\cos\bar{\sigma}\hat{\mathbf{e}}_{\bar{y}} + \sin\bar{\sigma}\hat{\mathbf{e}}_{\bar{z}}) \tag{18}$$

and thus

$$\hat{\mathbf{e}}_{\bar{\beta}} = \hat{\mathbf{e}}_{\bar{s}} \times \hat{\mathbf{e}}_{\bar{n}} = -\sin\bar{\sigma}\hat{\mathbf{e}}_{\bar{y}} + \cos\bar{\sigma}\hat{\mathbf{e}}_{\bar{z}} \tag{19}$$

Following the technique used in Ref. 1, Eqs. (18) and (19) are used to transform the $\bar{\xi}, \bar{n}, \bar{\beta}$ coordinates to $\bar{y}, \bar{z}, \bar{n}$ by the transformation operators

$$\frac{1}{\bar{h}_s}\frac{\partial}{\partial\bar{\xi}} = \sin\bar{\Gamma}\left[\cos\bar{\sigma}\frac{\partial}{\partial\bar{y}} + \sin\bar{\sigma}\frac{\partial}{\partial\bar{z}}\right] \tag{20}$$

and

$$(1/\bar{h})(\partial/\partial\bar{\beta}) = -\sin\bar{\sigma}(\partial/\partial\bar{y}) + \cos\bar{\sigma}(\partial/\partial\bar{z}) \tag{21}$$

The constant $\bar{\beta}$ curve on the shock wave follows from Eq. (20) as

$$\frac{\partial\bar{z}/\partial\bar{\xi}}{\partial\bar{y}/\partial\bar{\xi}} = \tan\bar{\sigma} = \frac{\bar{z}}{\bar{B}\bar{y}} \tag{22}$$

which integrates to

$$\bar{z}^{\bar{B}} = \bar{C}(\bar{\beta})\bar{y} \tag{23}$$

Note that the parameter $\bar{C}$ is a function of $\bar{\beta}$ only (on the shock wave).

Equation (23) can be differentiated to give

$$\partial\bar{\beta}/\partial\bar{y} = -\bar{C}/(\bar{C}'\bar{y}) \quad \text{and} \quad \partial\bar{\beta}/\partial\bar{z} = \bar{B}\bar{C}/(\bar{C}'\bar{z})$$
$$\text{where} \quad \bar{C}' = d\bar{C}/d\bar{\beta}.$$

Using these results, substitute $\bar{\beta}$ into the operator of Eq. (21) to obtain

$$\bar{h} = \frac{\bar{C}'}{\bar{C}^2}\frac{\bar{z}^{\bar{B}+1}}{[\bar{z}^2 + \bar{B}^2\bar{z}^{2\bar{B}}/\bar{C}^2]^{1/2}} \tag{24}$$

Now along the shock surface with $\bar{\beta}$ = constant, Eq. (20) can be used to give

$$d\bar{S} = (d\bar{z}/\bar{z})[\bar{z}^2 + \bar{B}^2\bar{z}^{2\bar{B}}/\bar{C}^2]^{1/2}/\sin\bar{\Gamma} \tag{25}$$

Finally, substitute Eqs. (24) and (25) into Eq. (5) to obtain

$$\Psi_{sh} = \frac{\bar{C}'}{\bar{C}^2}\frac{\bar{z}^{\bar{B}+1}}{(\bar{B}+1)}\rho_\infty V_\infty \tag{26}$$

The relation for the stagnation line shock standoff distance follows from Eq. (4) as

$$\Delta = \frac{1}{\bar{h}}\int_0^{\Psi_{sh}}\frac{d\Psi}{\rho\bar{u}} \simeq \frac{1}{\rho_2}\int_0^1\frac{d(\Psi/\Psi_{sh})}{(\bar{u}\bar{h}/\Psi_{sh})} \tag{27}$$

Along the stagnation lines both Ψ and Ψ_{sh} are zero. However, the ratio Ψ/Ψ_{sh} approaches a value in the range $0 \leqq \Psi/\Psi_{sh} \leqq 1$ in the limit as the stagnation line is approached ($\Psi/\Psi_{sh} = 1$ on the shock and $\Psi/\Psi_{sh} = 0$ on the body). Also, the ratio $\bar{u}\bar{h}/\Psi_{sh}$ is indeterminate along the stagnation line, and care must be exercised in evaluating this indeterminancy. The velocity component $\bar{u}$ is obtained from Eq. (11), but this equation must be rewritten in a form to facilitate the integration indicated in Eq. (27). Since the enthalpy is a function of the pressure and entropy, a Taylor series expansion about the position a streamline crosses the shock wave yields

$$h_e(\bar{\xi}, \bar{\beta}, \Psi) \simeq h_{sh}(\bar{\beta}, \Psi) + \left[\frac{\partial h_e}{\partial p}\right]_{sh}[p(\bar{\xi}, \bar{\beta}, \Psi) - p_{sh}(\bar{\beta}, \Psi)] \tag{28}$$

The arguments of these terms is illustrated in Fig. 5. For isentropic flow along a streamline, the Bernoulli and energy equations give

$$\left[\frac{\partial h_e}{\partial p}\right]_{sh} = \frac{1}{\rho_{sh}(\bar{\beta}, \Psi)} \tag{29}$$

With $\rho = \rho(p, h_e)$, the right-hand side of Eq. (29) is expressed by a Taylor series expansion about the normal shock position.

$$\frac{1}{\rho_{sh}(\bar{\beta}, \Psi)} \simeq \frac{1}{\rho_2} + \left[\frac{\partial(1/\rho)}{\partial p}\right]_2[p_{sh}(\bar{\beta}, \Psi) - p_2] + \left[\frac{\partial(1/\rho)}{\partial h_e}\right]_2[h_{sh}(\bar{\beta}, \Psi) - h_2] \tag{30}$$

The pressure for Eq. (28) is given by Eq. (9), and the derivatives on the right-hand side of Eq. (30) are evaluated from thermodynamic properties.[15]

Next, define

$$\sin^2\bar{\Gamma} \equiv 1 - G^2 \tag{31}$$

$$p_{sh} \equiv p_2 - \Delta p G^2 \tag{32}$$

$$h_{sh} \equiv h_2 - \Delta h G^2 \tag{33}$$

where near the stagnation line $G^2 \ll 1$. The parameters Δp and Δh depend only on the fluid properties aft of the normal shock wave and they are evaluated from the shock-wave relations.[15] Now, substitute Eqs. (29–32) into Eq. (28) and the resultant into Eq. (11). Neglecting the higher order terms the following result is obtained

$$\frac{\bar{h}^2u^2(\bar{\xi}, \bar{\beta}, \Psi)}{\Psi_{sh}^2} = \frac{2\Delta p}{\rho_2}\left[\frac{\bar{h}^2G^2(\bar{\xi}, \bar{\beta})}{\Psi_{sh}^2} + \left(\frac{\Delta h\rho_2}{\Delta p} - 1\right)\frac{\bar{h}^2G^2(\bar{\beta}, \Psi)}{\Psi_{sh}^2} + \frac{u_{sh}\bar{h}}{\bar{R}\Psi_{sh}}\frac{1}{\Delta p}\left(1 - \frac{\Psi}{\Psi_{sh}}\right)\right] \tag{34}$$

The square root of this equation is needed for the integral to determine the shock standoff distance.

Consider now the terms on the right side of Eq. (34). Substitute Eqs. (14) and (23) into (31) to obtain

$$G^2(\bar{\xi}, \bar{\beta}) \simeq (\bar{z}^2 + \bar{B}^2\bar{z}^{2\bar{B}}/\bar{C}^2)/\bar{R}_T{}^2 \tag{35}$$

This equation can also be used to obtain $G^2(\bar{\beta}, \Psi_{sh})$ by substituting for $\bar{z}$ in terms of Ψ_{sh} from Eq. (26). Then $G^2(\bar{\beta}, \Psi)$ follows from $G^2(\bar{\beta}, \Psi_{sh})$ by simply replacing Ψ_{sh} with Ψ. Now use these results along with Eqs. (24) and (26) to find the following parameters in the limit as the stagnation line is approached:

$$\bar{h}^2G^2(\bar{\xi}, \bar{\beta})/\Psi_{sh}{}^2 = (\bar{B}+1)^2/(\rho_\infty V_\infty \bar{R}_T)^2 \tag{36}$$

$$\bar{h}^2G^2(\bar{\beta}, \Psi)/\Psi_{sh}{}^2 = (\bar{B}+1)^2(\Psi/\Psi_{sh})^\wedge/(\rho_\infty V_\infty \bar{R}_T)^2 \tag{37}$$

where

$$\Lambda = \begin{cases} 2\bar{B}/(\bar{B}+1) & \text{for } 0 < \bar{B} \leqq 1 \\ 2/(\bar{B}+1) & \text{for } 1 < \bar{B} < \infty \end{cases} \tag{38}$$

$$\frac{\bar{u}_{sh}\bar{h}}{\bar{R}\Psi_{sh}} = \begin{cases} \bar{B}(\bar{B}+1)/(\rho_\infty \bar{R}_T{}^2) & \text{for } 0 < \bar{B} \leqq 1 \\ (\bar{B}+1)/(\rho_\infty \bar{R}_T{}^2) & \text{for } 1 < \bar{B} < \infty \end{cases} \tag{39}$$

Finally, substitute these results into Eq. (34) and then that result into Eq. (27) to obtain the shock standoff distance equation

$$\frac{\Delta}{\bar{R}_T} = \left[\frac{\rho_\infty V_\infty{}^2}{2\Delta p}\frac{\rho_\infty}{\rho_2}\right]^{1/2}\frac{1}{(\bar{B}+1)}\int_0^1\frac{d\eta}{[1 + D(1-\eta) + E\eta^\wedge]^{1/2}} \tag{40}$$

where $\eta = \Psi/\Psi_{sh}$,

$$D = \begin{cases} (\rho_\infty V_\infty{}^2/\Delta p)\bar{B}/(\bar{B}+1) & \text{for } 0 < \bar{B} \leqq 1 \\ (\rho_\infty V_\infty{}^2/\Delta p)/(\bar{B}+1) & \text{for } 1 < \bar{B} < \infty \end{cases} \quad (41a)$$

$$E = \rho_2 \Delta h/\Delta p - 1 \quad (41b)$$

For an ideal gas, it is shown in Ref. 15 that

$$\Delta p/(\rho_\infty V_\infty{}^2) = 2/(\gamma+1)$$

and

$$E = (M_\infty{}^2 - 1)/\{2M_\infty{}^2[1+(\gamma-1)/2(M_\infty{}^2)]\}$$

In general Eq. (40) cannot be integrated in closed form; however, for the special case of axisymmetric flow ($\bar{B} = 1$) it can be integrated to yield the same result given by Maslen.[13] For three-dimensional shocks, Maslen[14] found different shock standoff distances for different directions of approaching the stagnation line. Equation (40) gives a unique value for the standoff distance, and it gives results which compare very closely with the rms values of the numerical results obtained by Maslen[14] (see Ref. 15).

Shock Shape Downstream of Stagnation Region

Since the method given here is basically an inverse one, the entire shock shape in the subsonic-transonic region would normally have to be determined iteratively. However, it is assumed here that for a given surface pressure distribution the shock shape associated with each inviscid surface streamline can be calculated independently of the others. This procedure highly simplifies the calculations because inviscid surface streamlines are calculated in the method of Ref. 1.

For the region downstream of the stagnation line, it is assumed that $\bar{\beta} = \beta$, i.e., a constant $\bar{\beta}$ surface is assumed to intersect the body surface on a curve of constant β which is an inviscid surface streamline. With the approximation

$$\frac{\bar{u}_{sh}\Psi_{sh}}{\bar{R}\bar{h}} = -\frac{V_\infty \Psi_{sh}}{\bar{h}}\frac{\partial(\sin\bar{\Gamma})}{\partial\bar{S}} \simeq -\frac{V_\infty \Psi_{sh}}{h}\frac{\partial(\sin\bar{\Gamma})}{\partial S} \quad (42)$$

apply Eq. (9) on the body surface to obtain

$$\frac{\partial(\sin\bar{\Gamma})}{\partial S} = (p_b - p_{sh})\frac{h}{V_\infty \Psi_{sh}} \quad (43)$$

where h is the scale factor for the coordinate β on the body surface and S is distance along an inviscid surface streamline. This equation can be integrated numerically along an inviscid surface streamline to determine the value of $\sin\bar{\Gamma}$ (where $\bar{\Gamma}$ is the shock angle) associated with each position. The value of Ψ_{sh} corresponding to each position can be calculated numerically from Eq. (5) in the following form

$$\Psi_{sh} = \rho_\infty V_\infty \int_0 \sin\bar{\Gamma}\bar{h}\, d\bar{S} \simeq \rho_\infty V_\infty \int_0 \sin\bar{\Gamma} h\, dS \quad (44)$$

Equations (43) and (44) give $\bar{\Gamma}$ as a function of Ψ_{sh} and, as will be shown below, the value of $\bar{\Gamma}$ corresponding to a given value of Ψ_{sh} is all that is needed from the inviscid solution to determine the entropy at the edge of the boundary layer.

The surface pressure distribution used in Eq. (43) must be modified so that $p_b = p_{sh}$ at the stagnation line instead of the stagnation pressure. For a given surface pressure distribution which yields $p_e = p_s$ at the stagnation line, this can be accomplished by simply using

$$p_b = p_\infty + (p_e - p_\infty)\frac{(p_2 - p_\infty)}{(p_s - p_\infty)} \quad (45)$$

where p_b is the pressure to be used in Eq. (43) only.

Entropy at the Edge of the Boundary Layer

The mass flow per unit β within the boundary layer is

$$\Psi_{BL} = \rho_e \bar{u}_e h(\delta - \delta^*) \quad (46)$$

where $h\,d\beta$ is the spacing between inviscid surface streamlines. The method described in Ref. 1 will yield Ψ_{BL} along an inviscid surface streamline for a prescribed surface pressure distribution. Now the streamline at the edge of the boundary layer passed through the bow shock wave at the position where $\Psi_{sh} = \Psi_{BL}$ or, in other words, where the mass flow inside the boundary layer is equal to the mass flow entering a segment of the shock wave (see Fig. 2). For this value of Ψ_{sh}, the shock angle $\bar{\Gamma}$ is determined by the method devcloped in the previous section. After $\bar{\Gamma}$ is determined, the shock-wave relations give the entropy at the edge of the boundary layer. The entropy and surface pressure can then be used to calculate the other fluid properties at the boundary-layer edge.

Method for Calculating Heating Rates

For a three-dimensional body in hypersonic flow, the Newtonian stagnation point is located and the shock standoff distance and shock principal radii of curvature are calculated at the stagnation line from the following equations.[15]

$$\frac{R_T{}^2}{\bar{R}T^2} = \left[\frac{p_2 - p_\infty}{\rho_\infty V_\infty{}^2}\right]\left[1 - \frac{\Delta}{\bar{R}_T}\right]^2 \Big/ \left(\frac{\Delta p}{\rho_\infty V_\infty{}^2} + \frac{1}{\bar{B}+1}\right)$$

$$\frac{\bar{B}^2}{B^2} = \left[1 - \frac{\bar{B}\Delta}{\bar{R}_T}\right]^2\left[\frac{\Delta p}{\rho_\infty V_\infty{}^2} + \frac{1}{\bar{B}+1}\right]\Big/\left[1 - \frac{\Delta}{\bar{R}_T}\right]^2\left[\frac{\Delta p}{\rho_\infty V_\infty{}^2} + \frac{\bar{B}}{\bar{B}+1}\right]$$

An inviscid surface streamline is then traced from the stagnation point to a downstream position on the body by using a prescribed surface pressure distribution in the method of Ref. 1, but modified to include the entropy-layer swallowing effects. The modification amounts to adding Eqs. (43) and (44) to the integration routine to calculate $\bar{\Gamma}$ and Ψ_{sh} corresponding to this streamline. These two parameters are then used to calculate the entropy and other fluid properties at the edge of the boundary layer as described above. It should be noted that the streamline traced on the body is no longer an inviscid surface streamline since the properties at the edge of the body layer are used to calculate the geometry of this streamline. Thus, entropy-layer swallowing effects can change the geometry of the streamline and the scale factor h along that streamline.

At each position along a streamline heating rates are calculated by the method of Ref. 1 but using the new method for determining the properties at the edge of the boundary layer. Solutions are then computed along other streamlines until an adequate surface distribution is obtained.

Results and Discussion

All of the results presented in this paper were calculated for an ideal gas ($\gamma = 1.4$) and used the modified Newtonian pressure distribution. Figure 6 shows the laminar heat-transfer distribution in the windward plane of symmetry for a blunt 15° half-angle circular cone at $\alpha = 20°$, $M_\infty = 10.6$, $Re_{\infty,N} = 3.75 \times 10^4$, and $h_w/H_s = 0.27$. These results compare well with the experimental data; however the heating rates calculated with variable entropy at the edge of the boundary layer fall slightly below the results using normal-shock entropy. This trend is the reverse of that for

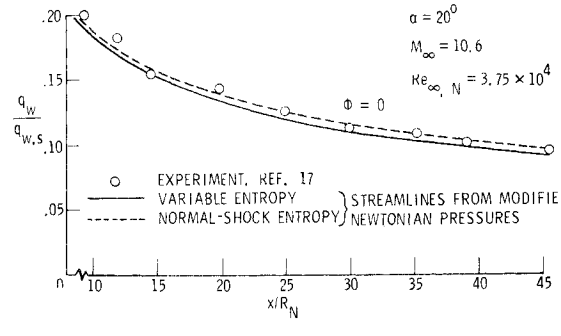

Fig. 6 Laminar heat-transfer distribution on blunt 15° half-angle cone.

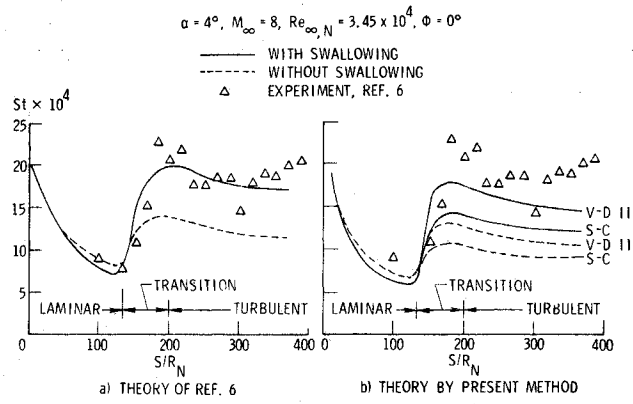

Fig. 7 Heat-transfer distribution on blunt 7.2° half-angle cone.

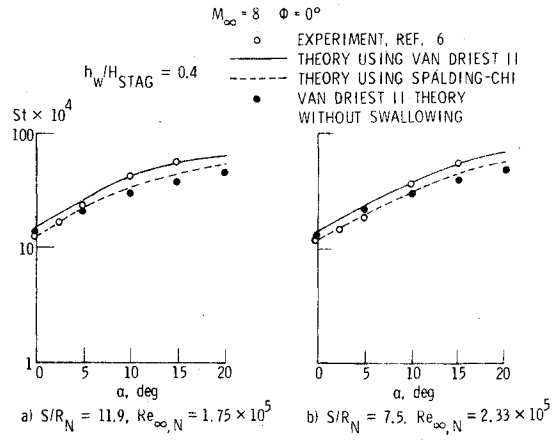

Fig. 9 Comparison of Stanton numbers computed from Van Driest II and Spalding-Chi methods for blunt 11° half-angle cone.

heating rates on axisymmetric bodies at $\alpha = 0$. Upon reviewing the present calculations it was found that near the windward plane of symmetry the inviscid streamlines at the edge of the boundary layer do not diverge nearly as much for the variable entropy solution as for the normal-shock entropy solution. The reduction in streamline spreading tends to reduce laminar heating rates, and here it more than compensates for the usual increase in heating rates due to entropy-layer swallowing.

Figure 7 shows comparisons of computed Stanton numbers in the windward plane of symmetry with experimental data for a blunt 7.2° half-angle cone at $\alpha = 4°$, $M_\infty = 8$, $Re_{\infty,N} = 34467$, and $h_w/H_s = 0.395$. Part a) gives the results calculated by Mayne,[6] and part b) gives the results calculated by the present method using the Spalding-Chi[10] and Van Driest II[16] methods for the turbulent heating. Mayne's method and the present method give higher laminar Stanton numbers without entropy-layer swallowing than with it, just as found in Fig. 6. On the other hand, the turbulent Stanton numbers are much higher with entropy-layer swallowing than without it. Streamline spreading has only a small effect on turbulent heating rates, and therefore entropy-layer swallowing effects increase turbulent heating rates.

Figure 7 also shows that for the present method the turbulent values calculated using the Van Driest II method[16] are much higher and closer to the experimental data than those using the Spalding-Chi method.[10] Mayne's results[6] compare more favorably with experimental data than the present results; however, part of the difference can be attributed to the inaccuracy of the modified Newtonian pressure distribution used in the present method.

Figure 8 shows Stanton numbers at two specified positions in the windward plane of symmetry for a blunt 11° half-angle cone at $M_\infty = 8$, $h_w/H_s = 0.4$, and angles of attack from 0 to 20°. (Here S is measured from the stagnation point at $\alpha = 0$.) Mayne's method[6] generally gives turbulent Stanton numbers somewhat higher and closer to the experimental data than the present method for angles of attack between 10° and 20°. The present method compares more favorably with experimental data for angles of attack less than 10°. Both methods include entropy-layer swallowing, and the present method used the Spalding-Chi technique for the turbulent calculations.

Figure 9 compares the turbulent Stanton numbers computed by the Van Driest II method with the Spalding-Chi method for the same conditions as Fig. 8. These results show the Van Driest II method to compare more favorably with experimental data for angles of attack between 10° and 20°, but the Spalding-Chi method was more accurate at angles of attack less than 10°. This figure also shows the reduction in the Stanton numbers when entropy-layer swallowing is neglected in the Van Driest II method.

The effects of entropy layer swallowing on the calculated turbulent Stanton number distribution along the windward plane of symmetry are shown in Fig. 10 for the same conditions as Fig. 9b. The effects of entropy-layer swallowing are large at $\alpha = 20°$ but small at $\alpha = 0$. The rise in the turbulent Stanton number for $\alpha = 20°$ (with entropy-layer swallowing) appears somewhat like a transition region. However, it is caused by the sharp drop in the shock angle where the streamline at the edge of the boundary layer crossed the shock wave, which is shown in Fig. 11. In contrast, the decrease in shock angle is shown to be relatively small for the $\alpha = 0$ case.

Figure 12 shows the laminar heating-rate ratio along the windward plane of symmetry of a blunted 2:1 elliptical cone

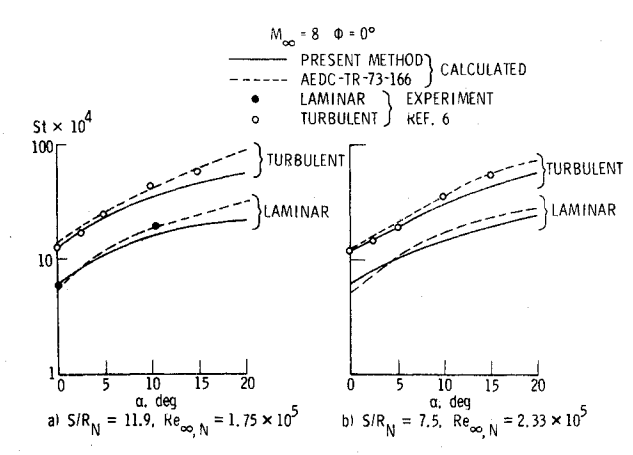

Fig. 8 Stanton numbers on blunt 11° half-angle cone.

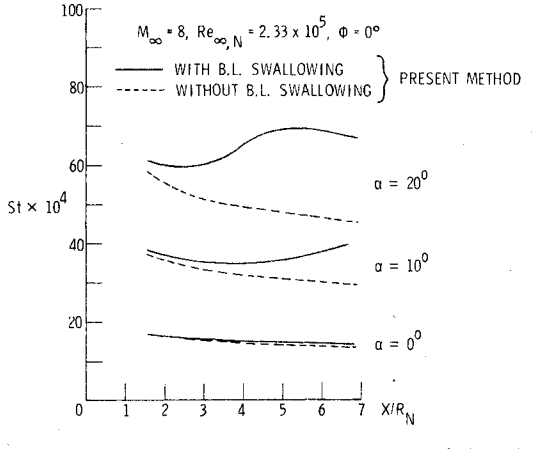

Fig. 10 Effects of entropy-layer swallowing on turbulent Stanton numbers for blunt 11° half-angle cone.

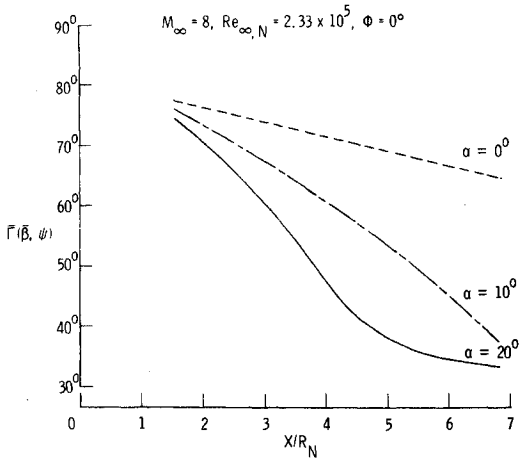

Fig. 11 Shock angle for streamline at boundary-layer edge on blunt 11° half-angle cone.

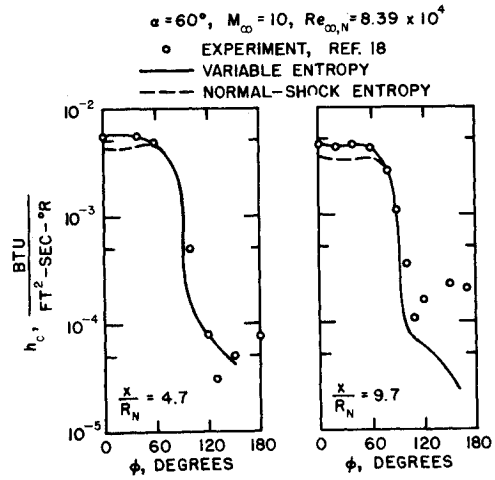

Fig. 13 Circumferential distribution of laminar heat-transfer coefficient on a blunt 2:1 elliptical cone.

(10° × 5 half angles) at $M_\infty = 10$, $Re_{\infty,N} = 8.39 \times 10^4$, and $\alpha = 15°$, 30°, and 60°. Since the windward surface here is flatter than the circular cone, the streamline divergence effect is smaller and hence the laminar heating rates are higher with entropy-layer swallowing than without it. Figure 13 illustrates the circumferential heat-transfer coefficient distribution and shows that entropy-layer swallowing effects are small away from the windward plane for this case.

Conclusions

A relatively simple and efficient method has been developed for including entropy-layer swallowing effects in the calculation of laminar, transitional, and turbulent heating on three-dimensional bodies in hypersonic flows. This method is not as sophisticated as Mayne's methods; however, his method is restricted to pointed circular cones or the windward plane of symmetry of axisymmetric bodies. Also, the inviscid solution must be obtained from some other method. In the present technique the inviscid solution is coupled with the viscous solution, and the method can be applied to general three-dimensional bodies. A typical case requires only about 7 sec of computational time per streamline on the IBM 370/165 computer.

The simple expression obtained for the three-dimensional shock standoff distance was found to compare well with Maslen's numerical results. For a blunted circular cone at an angle of attack, the laminar heating rates calculated with entropy-layer swallowing fell slightly below those calculated without it in the windward plane. This was attributed to the reduction in streamline spreading at the edge of the boundary layer with entropy layer swallowing, which reduces the laminar heating more than the usual increase in heating experienced by axisymmetric bodies at $\alpha = 0$. The elliptical cone has very little streamline spreading in the windward plane, either with or without entropy layer swallowing. Hence, the calculated laminar heating rates increased when entropy-layer swallowing effects were included.

Streamline divergence affects turbulent heating rates very little, and therefore large increases were observed in the calculated turbulent heating rates in the windward plane of a blunted cone when entropy-layer swallowing was included.

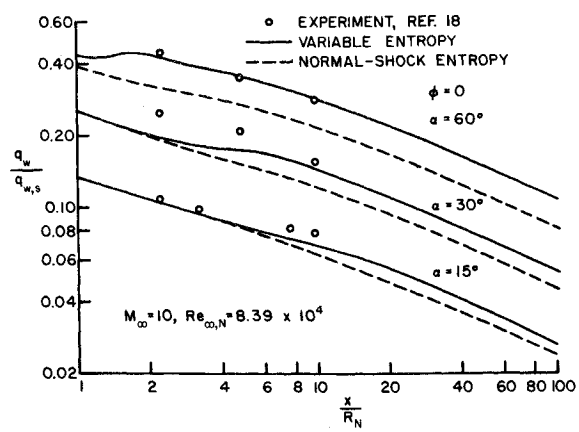

Fig. 12 Laminar heat-transfer distribution on a blunt 2:1 elliptical cone.

References

[1] DeJarnette, F. R. and Hamilton, H. H., "Inviscid Surface Streamlines and Heat Transfer on Shuttle-Type Configurations," *Journal of Spacecraft and Rockets*, Vol. 10, No. 6, May 1973, pp. 314–321.

[2] Mayne, A. W., Jr. and Adams, J. C., Jr., "Streamline Swallowing by Laminar Boundary Layers in Hypersonic Flow," AEDC-TR-71-32 (AD 719748), March 1971, Arnold Engineering Development Center, Tullahoma, Tenn.

[3] Ferri, A., "Some Heat Transfer Problems in Hypersonic Flow," *Aeronautics and Astronautics*, Pergamon Press, New York, 1960, pp. 344–377.

[4] Mayne, A. W., Jr. and Dyer, D. F., "Comparisons of Theory and Experiment for Turbulent Boundary Layers on Simple Shapes at Hypersonic Conditions," *Proceedings of the 1970 Heat Transfer and Fluid Mechanics Institute*, Stanford University Press, 1970, pp. 168–188.

[5] Mayne, A. W., Jr., "Analysis of Laminar Boundary Layers on Right Circular Cones at Angle of Attack, Including Streamline-Swallowing Effects," AEDC-TR-72-134 (AD 750130), Oct., 1972, Arnold Engineering Development Center, Tullahoma, Tenn.

[6] Mayne, A. W., Jr., "Calculation of the Boundary-Layer Flow in the Windward Symmetry Plane of a Spherically Blunted Axisymmetric Body at Angle of Attack, Including Streamline-Swallowing Effects," AEDC-TR-73-166, Oct. 1973, Arnold Engineering Development Center, Tullahoma, Tenn.

[7] Jones, D. J., "Numerical Solutions of the Flow Field for Conical Bodies in a Supersonic Stream," NRC Aeronautical Rept. LR-507, Ottawa, Canada, July 1968.

[8] Rakich, J. V., "A Method of Characteristics for Steady Three-Dimensional Supersonic Flow with Application to Inclined Bodies of Revolution," TN D-5341, Oct. 1969, NASA.

[9] Beckwith, I. E. and Cohen, N. B., "Application of Similar Solutions to Calculation of Laminar Heat Transfer on Bodies With Yaw and Large Adverse Pressure Gradient in High-Speed Flow," TN D-625, 1961, NASA.

[10] Spalding, D. B. and Chi, S. W., "The Drag of a Compressible

Turbulent Boundary Layer on a Smooth Flat Plate With and Without Heat Transfer," *Journal of Fluid Mechanics*, Vol. 18, Pt. 1, Jan. 1964, pp. 117–143.

[11] Reshotko, E. and Tucker, M., "Approximate Calculation of the Compressible Turbulent Boundary Layer With Heat Transfer and Arbitrary Pressure Gradient," TN 4154, 1957, NACA.

[12] Dhawan, S. and Narasimha, R., "Some Properties of Boundary Layer Flow During the Transition From Laminar to Turbulent Motion," *Journal of Fluid Mechanics*, Vol. 3, No. 4, April 1958, pp. 418–436.

[13] Maslen, S. H., "Inviscid Hypersonic Flow Past Smooth Symmetric Bodies," *AIAA Journal*, Vol. 2, No. 6, June, 1964, pp. 1055–1061.

[14] Maslen, S. H., "Asymmetric Hypersonic Flow," CR-2123, Sept. 1972, NASA.

[15] DeJarnette, F. R., "Calculation of Heat Transfer on Shuttle-Type Configurations Including the Effects of Variable Entropy at Boundary Layer Edge," CR-112180, Oct. 1972, NASA.

[16] Hopkins, E. J. and Inouye, M., "An Evaluation of Theories for Predicting Turbulent Skin Friction and Heat Transfer on Flat Plates at Supersonic and Hypersonic Mach Numbers," *AIAA Journal*, Vol. 9, No. 6, June, 1971, pp. 993–1003.

[17] Cleary, J. W., "Effects of Angle of Attack and Bluntness on Laminar Heating-Rate Distributions of a 15° Cone at a Mach Number of 10.6," TN D-5450, 1969, NASA.

[18] Hillsamer, M. E., and Rhudy, J. P., "Heat-Transfer and Shadowgraph Tests of Several Elliptical Lifting Bodies at Mach 10," U.S. Air Force, AEDC-TDR-64-19, 1964, Arnold Engineering Development Center, Tullahoma, Tenn.

JANUARY 1975 J. SPACECRAFT VOL. 12, NO. 1

High Angle-of-Attack Aerodynamics on a Slender Body with a Jet Plume

R. C. NELSON* AND E. L. FLEEMAN†
Air Force Flight Dynamics Laboratory, Wright-Patterson Air Force Base, Ohio

This paper presents an aerodynamic analysis of data obtained from recent wind-tunnel tests on a slender body configuration. Force and moment coefficients are presented for angles of attack up to 180°, Mach numbers up to 2.2, and Reynolds numbers (based on diameter) up to 10^6. The rocket exhaust plume was simulated by exhausting cold air (ambient total temperature) through the nozzle of the model. This permitted study of the plume interference effects on the aerodynamic coefficients. The jet effects on normal force were found to be important when the angle of attack exceeded 40° in subsonic flow and 90° in supersonic flow. Deflecting the nozzle at high angles of attack also caused large excursions in the center-of-pressure location. Another problem associated with high angle-of-attack flight is the appearance of large side forces and yawing moments for a symmetric flight condition. These are due to steady asymmetric shedding of the body vortices. Data are presented which illustrate the influence of Mach number and Reynolds number on the out-of-plane forces.

Nomenclature

A = cross-sectional area of cylindrical portion of the body
A_b = body base area
A_p = planform area
C_{d_n} = cross-flow drag coefficient of cylinder, $F_n/(q_n \Delta l_{cy} d)$
C_m = pitching moment coefficient, $M/(qAd)$ (positive nose up)
C_n = yawing moment coefficient, $N/(qAd)$ (positive nose to the right)
C_N = normal force coefficient, $F_n/(qA)$
C_Y = side force coefficient, $Y/(qA)$
ΔC_N = $C_{N\,\text{jet on}} - C_{N\,\text{jet off}}$
d = model diameter or circular cylinder diameter
d_{NT} = nose tip diameter
F_n = normal force
l = body length
l_{cy} = cylinder length
l_N = nose length
M = pitching moment or Mach number
N = yawing moment
P_{t_j} = total pressure of the jet
P_{t_∞} = total pressure of the freestream
q = dynamic pressure
q_n = cross-flow dynamic pressure
R_{e_d} = Reynolds number based on model diameter
U = free-stream velocity
X_{cp} = location of center-of-pressure from the model nose
X_{cg} = location of center-of-gravity from model nose, 8.4d
Y = side force
α = angle-of-attack
β = angle-of-sideslip
δ = nozzle deflection (positive deflection into the wind)
η = cross-flow drag proportionality factor

Presented as Paper 74–110 at the AIAA 12th Aerospace Sciences Meeting, Washington, D.C., January 30–February 1, 1974; submitted February 21, 1974; revision received August 2, 1974. The authors gratefully acknowledge assistance by J. Jones (ARO, Inc.), D. Shereda (AFFDL), D. Perper (Hughes Aircraft), J. Donahoe (Martin Orlando), and E. Chambers (Raytheon Missile Systems Division) for efforts in supporting schlieren photography, computer calculations, and model and balance construction.

Index category: Missile Aerodynamics.

* Aerospace Engineer, Control Criteria Branch, Flight Control Division. Member AIAA.

† Aerospace Engineer, Control Criteria Branch, Flight Control Division. Member AIAA.

Introduction

IN recent years tactical aircraft and missiles have been designed with increased emphasis on achieving more maneuverability. As a result of this design trend, aircraft and missiles are flying at much higher angles of attack than in the past. In fact, there are designs presently under consideration for missiles which will fly at angles of attack ranging from 0°–180°. The design of such highly maneuverable missiles has prompted a renewed interest